APPLIED SCIENCES AND ENGINEERING

Hydrogel 3D printing with the capacitor edge effect

Jikun Wang*, Tongqing Lu*, Meng Yang, Danqi Sun, Yukun Xia, Tiejun Wang†

Recent decades have seen intense developments of hydrogel applications for cell cultures, tissue engineering, soft robotics, and ionic devices. Advanced fabrication techniques for hydrogel structures are being developed to meet user-specified requirements. Existing hydrogel 3D printing techniques place substantial constraints on the physical and chemical properties of hydrogel precursors as well as the printed hydrogel structures. This study proposes a novel method for patterning liquids with a resolution of 100 µm by using the capacitor edge effect. We establish a complete hydrogel 3D printing system combining the patterning and stacking processes. This technique is applicable to a wide variety of hydrogels, overcoming the limitations of existing techniques. We demonstrate printed hydrogel structures including a hydrogel scaffold, a hydrogel composite that responds sensitively to temperature, and an ionic high-integrity hydrogel display device. The proposed technique offers great opportunities in rapid prototyping hydrogel devices using multiple compositions and complex geometries.

INTRODUCTION

Hydrogels are three-dimensional (3D) polymer networks that can retain a large amount of water in their swollen states. Over recent decades, hydrogels have been widely used in bioengineering and daily life owing to their excellent biocompatibility (1). Applications include contact lenses (1), diapers (2), drug delivery (3), cell culture (4), and tissue engineering (4–6). Recently, the invention of functional hydrogels, such as responsive hydrogels (7, 8), double-network hydrogels (9), and tough hydrogels (10), has greatly expanded applications to soft sensors (11), actuators (7, 8, 12, 13), and stretchable ionic devices (14–17). The intense developments in hydrogel applications call for advanced techniques for fabricating complex hydrogel structures.

3D printing has become an effective tool for fabricating highly ordered, interconnected, and porous hydrogel structures compared to conventional methods such as casting, photomasking, and electrospinning (18, 19). People have used 3D printing to fabricate highly porous hydrogel scaffolds for cell cultures (5, 20, 21), biomimetic microchips for studying cancer metastasis (22), artificial heterogeneous tissues and organs with high geometric precision and biocompatibility (18, 23), and highly elastic, transparent, and conductive hydrogel composites for soft robotics (24, 25). In particular, for applications in tissue engineering, computer-aided design in 3D printing is suitable for building highly programmed and user-specified hydrogel structures (5, 26).

Digital projection lithography (DLP), stereolithography (SLA), and direct ink writing (DIW) are commonly used techniques for printing hydrogels (26). In DLP, hydrogel structures are fabricated through a pull-out procedure from a hydrogel precursor with the aid of photo-patterned crosslinking (5, 20, 26). In SLA, the precursors are selectively photopolymerized by a laser layer by layer (27). These two printing methods enable high-speed processing of hydrogels with very high resolution, which ranges from 10 to 100 µm (20, 26). However, they are limited to patterning with photopolymerizable hydrogel precursors (26). One way to increase photoinitiator (PI) content is to mix poorly water-soluble PIs with hydrogel precursors through agitation or heating or using organic solvents (28); the other way is to transform poorly water-soluble PIs into highly water-dispersible PI nanoparticles by surface modification (20). DIW deposits hydrogel precursors through positioned ejection from a movable print head. The resolution of DIW is usually lower than that of DLP and SLA, which ranges from 100 µm to 1 mm; nevertheless, DIW provides higher degrees of flexibility in choosing different types of hydrogels and can print multiple hydrogels simultaneously (18, 26). However, the hydrogel precursor is water-like and difficult to deposit. To increase the viscosity of the precursor, nanoclays must be added (18) or pre-crosslinking must be done before deposition (22, 24, 29). Moreover, the velocity of the extruded precursors and the velocity of nozzle movement need to be well controlled to match the viscosity of the precursor. The mechanical properties of DIW-printed objects are usually greatly affected by the processing mentioned above (5, 29).

Electric fields have been used to control liquids in many research fields such as electrowetting (30), dielectrophoresis (31), and lithographically induced self-assembly (32). These techniques are used to control single droplets between two electrodes to dispense, mix, transport, position, and pattern, finding many applications in cell cultures (33), patterned wettability (34), microfluidics devices (35), and patterning electronics (32). However, the abovementioned techniques of patterning liquids using electric fields can only manipulate a single droplet at a time. The lack of massive-scale control of liquid droplets makes it very difficult to use them for 3D printing. Moreover, the effective controllable zone only concentrates on the narrow region between the two electrodes, which makes it impossible to form a 3D object by stacking.

Here, we propose a novel method of patterning liquids with the capacitor edge effect (PLEEC). This method can pattern a wide variety of hydrogel solutions with different physical and chemical properties. It is also applicable for different crosslinking mechanisms and crosslinking of multiple materials. The asymmetric design of the capacitor makes it possible to build a real 3D object rather than merely 2D patterns within two electrodes. We build a 3D printing system based on the new method and demonstrate a series of printed hydrogel structures including a hydrogel scaffold, a hydrogel composite, and hydrogel ionic devices.

RESULTS

Patterning liquid with the capacitor edge effect

When a parallel capacitor is charged, most of the electric field concentrates in the region between the two electrodes. The electric field

State Key Lab for Strength and Vibration of Mechanical Structures, Department of Engineering Mechanics, Xi'an Jiaotong University, Xi'an 710049, China.
*These authors contributed equally to this work.
†Corresponding author. Email: wangtj@mail.xjtu.edu.cn

lines distort at the edges of the capacitor, and a small portion of the electric field exists in the outer space of the capacitor, which is called the capacitor edge effect. For a symmetric capacitor, i.e., where the upper and lower electrodes are of equal size, the edge effect is very weak. However, for an asymmetric capacitor, the edge effect can be greatly strengthened. We compare the differences in distributions of the electric field for symmetric and asymmetric capacitors using finite element calculations (fig. S1). We propose using the asymmetric design to trap and control liquids in an open space.

The proposed PLEEC panel consists of five layers (Fig. 1). A pair of electrodes made of silver adhesives is separated by a dielectric layer (polyimide film). The upper electrode has a smaller size than the lower electrode. The three layers form an asymmetric capacitor, which is the key feature of our design. At the bottom is the substrate made of insulating material (acrylate film). The top layer (Teflon film) acts as an insulating cover to separate the liquid on the top from the upper electrode. The top layer is chosen to be hydrophobic so that any liquid on the top tends to flow away in the absence of an electric field. Upon applying an electric field, the edge effect generates electrostatic force to trap the liquid on top of the hydrophobic layer. We calculate the change of Helmholtz free energy of the PLEEC system when a drop of liquid is placed on the top layer (fig. S2). We find that the asymmetric design greatly amplifies the capacitor edge effect and thus can trap the liquid firmly in competition with its surface energy. In the optimal design for the asymmetric capacitor, the size of the upper electrode is roughly half of the lower electrode's size (fig. S2). The capacitor lies on an insulated substrate and is covered by a hydrophobic layer. When the capacitor is charged, the electric field induced by the edge effect is strong enough to trap the liquid on top of the hydrophobic layer.

Using the principle above, we design liquid patterns with different shapes and sizes. The upper electrode is connected to the positive pole, and the lower electrode (with double the width of the upper electrode) is connected to the negative pole. When a voltage is applied, the liquid within regions with exactly the same shape and size as the lower electrodes is trapped owing to the capacitor edge effect (Fig. 2A). Figure 2 (B and C) shows the trapped blue ink forming patterns of an angry bird and the letters "XJTU." Figure 2D shows an array of line pixels, each of which can be controlled to trap liquid independently. Each unit with seven line pixels is capable of displaying nine natural numbers. For example, if we want to display the number "1," we only apply voltage to the two pixels on the right. Figure 2E shows an array of 10×10 dot pixels with more flexibility to form various liquid patterns such as lines, squares, and musical notes. With maturely developed circuit control technology, more complicated liquid patterns can be designed and controlled. The pixel design eliminates the limitation of electrode shape and greatly strengthens the applicability of the proposed PLEEC method.
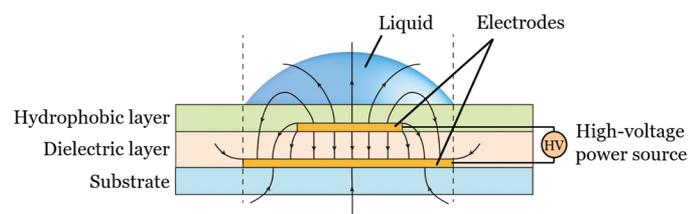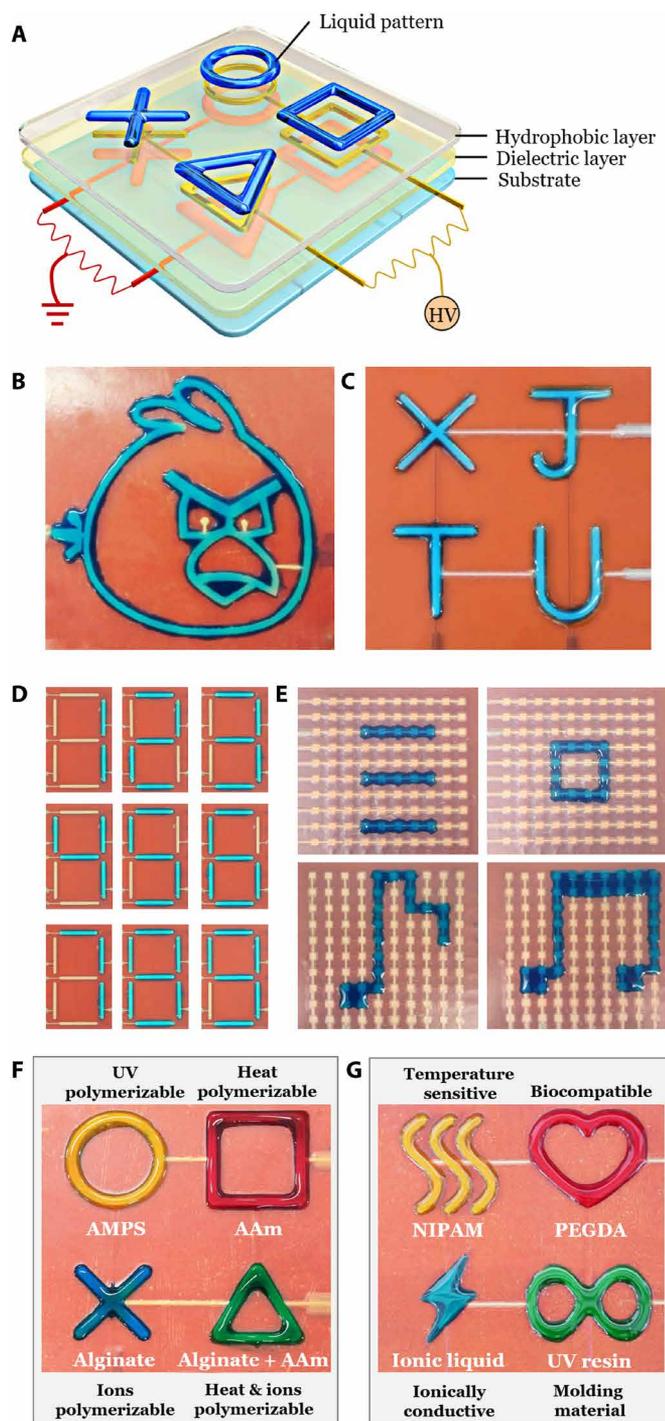
Figure 2F shows four representative hydrogel precursors trapped by the electric field. The yellow circle shows the trapped 2-acrylamido-2-methylpropanesulfonic acid (AMPS) solution, which is then polymerized into PAMPS hydrogel by ultraviolet (UV) light. The red square shows the trapped acrylamide (AAm) solution, which is then polymerized into PAAm hydrogel by heat. These two hydrogel precursors are water-like and therefore very difficult to control through other methods. The blue cross shows the alginate solution, which is then polymerized into a brittle alginate hydrogel by ion exchange. The green triangle shows the alginate/AAm solution, which is then polymerized into an alginate/PAAm tough hydrogel by heat and ion exchange. These two precursors are relatively viscous aqueous solutions; their viscosity is about 2800 mPa·s. We use Teflon as the top layer of the PLEEC panel, which is hydrophobic and slippery, so that the shape of the viscous solutions can be controlled precisely. This demonstrates the diverse applicability of hydrogel 3D printing, which greatly reduces the chemical and physical requirements of hydrogel precursors.

We can also trap functional materials using the electric field apart from other hydrogel precursors (Fig. 2G). The yellow wavy lines are a *N*-isopropyl acrylamide (NIPAM) solution, which can be polymerized into temperature-sensitive PNIPAM hydrogels (13). The red heart is a polyethylene glycol diacrylate (PEGDA) solution, which is widely used in bioengineering applications (18). The blue flash shows the trapped ionic liquid, which is ionically conductive and nonvolatile. Ionic hydrogels made of ionic liquid have been demonstrated as good candidates for stretchable ionic conductors (36). The green loop shows the trapped photosensitive resin, which is one of the most widely used molding or insulating materials in 3D printing. Figure 2 (F and G) shows that the PLEEC technique is capable of trapping a wider variety of liquid solutions and offers potential opportunities for massive-scale liquid manipulation, flexible displays, transfer printing, and hydrogel 3D printing.
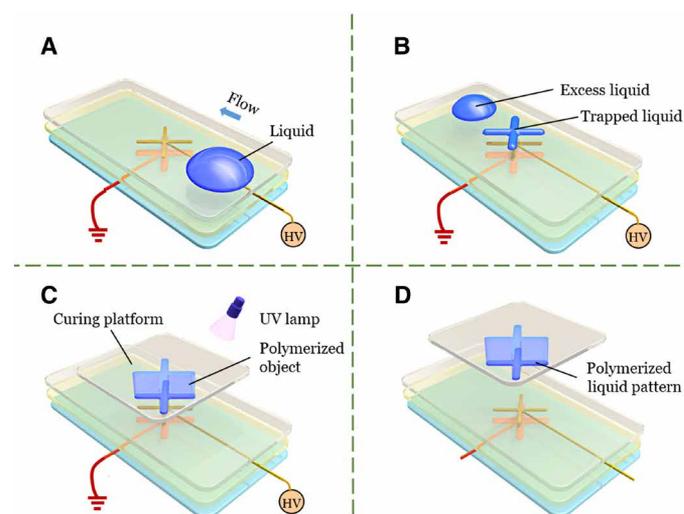
When the liquid is trapped on the PLEEC panel, the electrical energy competes with the surface energy. According to dimensional analysis, the characteristic size of the PLEEC panel, that is, the smallest length scale of the liquid that can be trapped, is proportional to $\gamma/(\varepsilon E^2)$, where γ is the surface energy of the liquid per unit area, ε is the dielectric constant of the environment, and E is the maximal electric field in the space, which is limited by the breakdown strength of air. εE^2 is the electrical energy density per unit volume. For aqueous solutions in the air, $\gamma = 7.3 \times 10^{-2}$ N/m, $\varepsilon = 8.9 \times 10^{-12}$ F/m, and $E = 3.0 \times 10^6$ V/m; we estimate the characteristic size of the PLEEC panel as being on the order of a millimeter (fig. S3A). To further increase the resolution, we can increase the dielectric constant ε and the maximal electric field E or decrease the surface energy of the liquid γ. For example, we can add some surfactant to the aqueous solution to decrease the surface energy. As a result, a line of water with a width of 100 μm can be trapped by the electric field (see fig. S3B). This resolution is very close to that of DLP and SLA.

Hydrogel 3D printing with PLEEC

Figure 3 shows how 2D hydrogel precursor patterns are polymerized and then stacked layer by layer into a 3D structure. When liquids flow over the designed electrodes, the liquid patterns are trapped by the electric field and excess liquid flows away (Fig. 3, A and B). In the printing plane, the in-plane size of the trapped liquid is determined by the lower electrode. When the material parameters are given, the thickness of the trapped liquid can be calculated from the


Fig. 1. Principle of PLEEC. An asymmetric capacitor is separated by a dielectric layer.

Fig. 3. Hydrogel 3D printing process with PLEEC. (**A** and **B**) Patterning process. When liquids flow over the designed electrode, the liquid patterns are trapped by the electric field. (**C**) Polymerization process. The curing platform moves down to contact the liquid pattern, and the hydrogel solution is polymerized by UV light. (**D**) Resetting process. The curing platform moves upward together with the newly formed hydrogel layer.

Fig. 2. Demonstrations of PLEEC. (**A**) Asymmetric capacitors with different shapes. The lower electrodes have double the widths of the upper electrodes. When the voltage is on, the liquid is trapped within the patterned region of the lower electrodes. (**B**) Liquid pattern in the shape of an angry bird. (**C**) Liquid pattern of four letters "X," "J," "T," and "U." (**D**) Liquid patterns of nine natural numbers by independently controlling line pixels. (**E**) Changeable liquid patterns in the same PLEEC panel by independently controlling 10×10 pixels. (**F**) Liquid patterns of four representative hydrogel precursors with different chemical and physical properties and polymerization into hydrogel by different polymerization methods. (**G**) Liquid patterns of four functional materials: temperature sensitive, biocompatible, ionically conductive, and molding materials. Photo credit: Jikun Wang, Xi'an Jiaotong University.

geometry shown in Fig. 1. In our experiment, the thickness ranged from one-fourth to one-half of the in-plane size. A transparent curing platform with previously polymerized materials approached the liquid pattern and attached it (Fig. 3C). During this process, the hydrogel solution was polymerized, for example, by UV light, to form a new layer of hydrogel. The newly formed layer became part of the polymerized materials by natural bonding. In the next step, as the curing platform moved upward, the new hydrogel layer adhered to the previously polymerized materials and detached from the PLEEC panel. No remaining hydrogel was left on the panel, and the next cycle started (Fig. 3D). The printing speed of the PLEEC method is determined by the time of liquid patterning and the time of polymerization. In our experiment, the time of liquid patterning is on the order of 10^1 s and the time of polymerization is on the order of 10^2 s, which is nearly comparable to the existing DLP technique.

We designed a hydrogel 3D printing system using the PLEEC technique. The system consists of seven parts: a mechanical module, a PLEEC panel, a solution-adding unit, a curing platform, a curing unit, a power supply, and a control module (Fig. 4A). Two orthogonally aligned slide guide rails are fixed onto the supporting platform. The PLEEC panel is horizontally fixed on the sliding block of the upper guide rail and can move in the x-y plane. The solution-adding unit, which is connected to a solution tank, is fixed on the shell of the upper guide rail. The hydrogel solutions are squeezed onto the PLEEC panel through the solution-adding holes. The hydrogel solutions are guided by blades to flow all over the panel. The thickness of the liquid layer is determined by the distance between the blades and the PLEEC panel (fig. S4). The leading speed should match the viscosity of the liquid. In printing hydrogel devices, the viscosities of hydrogel precursors are all below 1000 mPa·s, and the patterns form fairly well. The curing platform is above the PLEEC panel and is fixed on a vertical slide guide rail that moves in the z direction. A curing unit such as a UV lamp or heating plate can be fixed on the curing platform at an appropriate location. The power
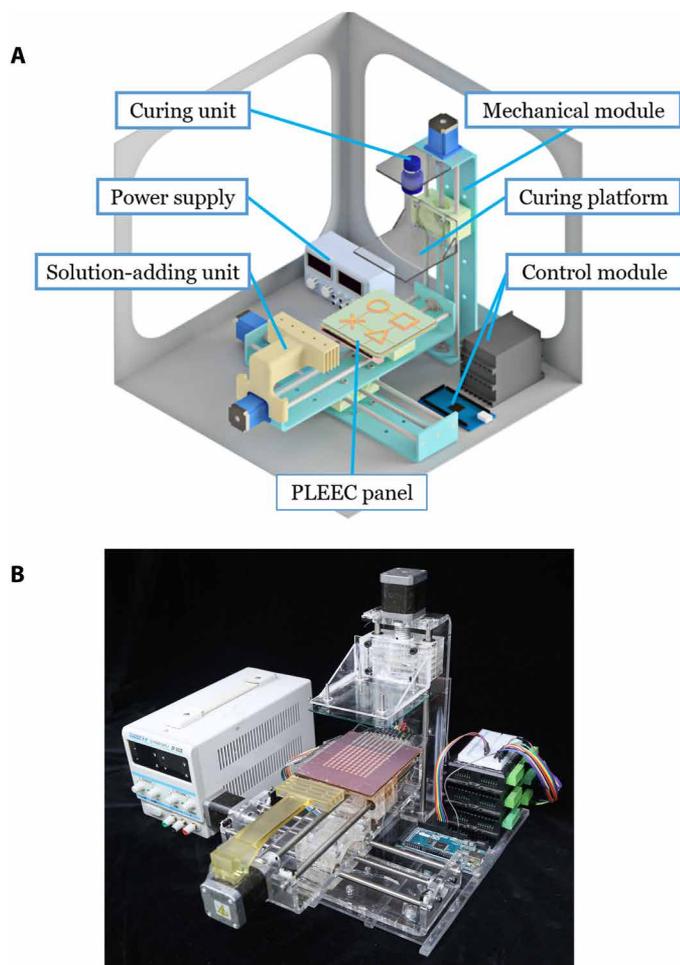
Fig. 4. Hydrogel 3D printing system with PLEEC. (**A**) System schematic. The system consists of seven parts: a mechanical module, a PLEEC panel, a solution-adding unit, a curing platform, a curing unit, a power supply, and a control module. (**B**) Our in-house printing system. Photo credit: Jikun Wang, Xi'an Jiaotong University.

supply provides low voltage for the mechanical movement module and high voltage for the PLEEC panel. The movement of each guide rail and the applied voltage are controlled by the control unit. The control module receives instructions from the computer and sends signals to all the other units. Figure 4B shows our in-house printing system. The system is controlled by a single chip (Arduino Mega 2560 R3). Three 42-stepper motors are controlled by Leadshine DM542 to actuate the three sliding rails. The high voltage is generated by a high-voltage power supply (Trek 610E). In this work, the voltage applied to the PLEEC panel is 3000 V at 1 kHz.

3D printed hydrogel structures

We form liquid patterns using three line pixels in the x direction and another three in the y direction. Hydrogel solution lines in the two directions are polymerized and stacked alternately to form a scaffold-structured hydrogel solid (Fig. 5A). We also form liquid patterns with 10×10 dot pixels and print two different musical notes (Fig. 5A). We next design a hydrogel composite using PAAm hydrogel and PNIPAM hydrogel. We polymerize one layer of PAAm hydrogel in the shape of a human hand as the first layer. Then, we polymerize PAAm hydrogel and PNIPAM hydrogel in different re-

gions for the five fingers as the second layer on top of the first layer (Fig. 5, B and C). The thickness of the second layer is double that of the first layer. The fabricated hydrogel composite is transparent and flat at room temperature. We dye it a blue color. When we put the hand-shaped hydrogel composite into hot water, the temperature-sensitive PNIPAM hydrogel tends to shrink so that the double-layered structure rolls up. Figure 5B shows that the four fingers roll up to form a gesture of "GOOD." Figure 5C shows that the thumb and index finger roll up to form a gesture of "OK."

Hydrogels can be used as transparent, ionic, and stretchable conductors (*14*). Novel ionic devices made of hydrogels have been developed more recently such as ionic cable, ionic music, ionic touch panels, and ionic adhesives (*37*). Assembling ionic and electronic components into a hydrogel ionotronic device is challenging and usually requires multiple steps. Molds are often used to prepare hydrogels, and reserved space is needed for subsequent injection of hydrogel solutions. In particular, bonding properties are always a concern in combining hard and soft components. These requirements make it difficult for light- and nozzle-based methods to 3D-print ionic hydrogel devices. In the present printing process, when the hydrogel solution patterns are formed on the PLEEC panel, other components can be assembled together on the panel with their pins immersed in the hydrogel solution. After the curing process, the components naturally become part of the hydrogel device with high integrity and excellent bonding.

We polymerized two lines of AAm hydrogel precursor and printed them onto a polymeric dielectric substrate (Fig. 5D). The substrate is made of very high bond (VHB) material (3 M), which is transparent and stretchable. Before curing, the lead pins of the light-emitting diodes (LEDs) were directly immersed in the two solution lines. After a single step of curing, the stretchable LED belt was fabricated. The interlaminar strength between two printed layers of the light-curable PAAm hydrogel was measured to be 56.9 N/m by a peeling test. The fracture strength of the bulk PAAm hydrogel material was measured to be 66.9 N/m. The interface between the VHB material and hydrogel and the interface between LED pins and hydrogel were treated following the methods in the literature (*38*, *39*). When an alternate voltage was applied to the two hydrogel electrodes, the LED illuminated. The LED worked well, even when the belt was stretched to double its original length after 100 loading cycles. Its good cyclic properties are attributed to the soft nature of the integrated device and its excellent bonding, which benefits from the one-step assembly process. Figure 5E shows a 3D display device with four hydrogel pillars as electrodes and four LEDs in between. Each LED with a different color can be controlled independently. After curing, the whole structure was sealed with polydimethylsiloxane to increase its integrity.

DISCUSSION

In summary, we proposed a novel design of a PLEEC panel to generate complex liquid patterns. We used this method to set up a 3D printing system for additively manufacturing hydrogel structures and demonstrated the printed hydrogel lattice, hydrogel composite, and hydrogel display device. This technology has several advantages compared to existing methods for hydrogel 3D printing. First, a wide range of hydrogels with different physical or chemical properties can be printed. The hydrogels can be highly viscous or less viscous and physically bonded or chemically bonded. The methods of polymerization can be heat curing, UV curing, or ion-exchange curing. Second,
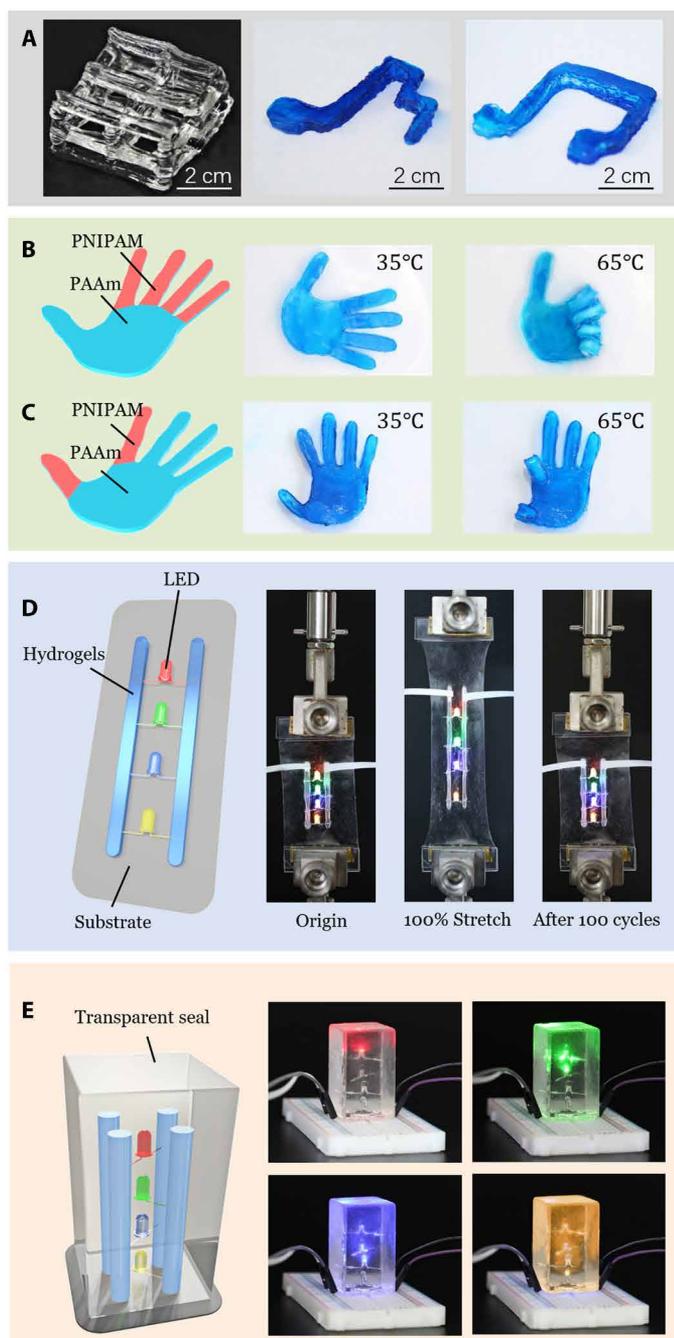
Fig. 5. Printed hydrogel structures using the PLEEC system. (A) Scaffold-structured hydrogel lattice. (**B** and **C**) PAAm and PNIPAM hydrogel composites. When the polymerized hydrogel composite is placed in hot water, the PNIPAM hydrogel tends to shrink so that fingers roll up. (**D**) Stretchable LED belt. LEDs work well when the belt is stretched to double its length and suffers 100 loading cycles. (**E**) Soft display device. Each LED can be lit independently. Photo credit: Jikun Wang, Xi'an Jiaotong University.

multiple hydrogel materials can be easily patterned to form hydrogel composites such as soft and hard mixtures, active and passive mixtures, and multifunctional composites. Last, in assembling ionically conductive hydrogels with electronically conductive components, the one-step curing process brings great benefits such as excellent integrity and bonding properties.

The precision of our printing technique can be further improved if a dielectric layer with higher permittivity is used or if the apparatus is immersed in an environment with higher electrical breakdown strength. The activation voltage can also be markedly decreased if a more advanced technique is used to fabricate a much thinner layer. If the pixel size can be further decreased to micrometer scale or smaller, this printing technique has great potential to print very complex and precise hydrogel structures such as artificial tissues, soft metamaterials, soft electronics, and soft robotics.

MATERIALS AND METHODS
Numerical simulations
We used COMSOL (Multiphysics 5.3) to simulate the distribution of the electric field in the vicinity of the capacitor in the absence of liquid (fig. S1). The capacitor was located in a large open space. In the simulation, we used the same parameters as those in the experiments. For the symmetric capacitor, the upper and lower electrodes had the same radius of 2 mm. For the asymmetric capacitor, the radius of the upper electrode was changed to 1 mm. All other parameters for the two capacitors were the same: The thicknesses of the electrode, dielectric layer, and hydrophobic layer were 0.06, 0.1, and 0.08 mm, respectively. The relative permittivity values of the dielectric and hydrophobic layers were 4 and 3, respectively. The applied voltage was 3000 V.

The Helmholtz free energy of the system consists of the electrostatic energy of the capacitor, the surface energy, and the free energy of the battery. We calculated the difference in free energy of the system before and after a drop of liquid was placed on the top of the hydrophobic layer. If $\Delta F < 0$, the system tends to trap the liquid; if $\Delta F > 0$, the liquid tends to flow away. The surface energies of water and air, Teflon and air, and Teflon and water are 0.07, 0.03, and 0.055 J m^{-2}, respectively. We found that ΔF was positive for the symmetric capacitor and negative for the asymmetric capacitor, which indicated that asymmetric capacitors could capture liquid effectively. We varied the size ratio of the upper electrode to the lower electrode to optimize the design. The calculated maximal change of free energy corresponds to a ratio of about 0.6 (fig. S2). With the given parameters, the minimum size of liquid that the PLEEC panel can trap was calculated to be on the order of a millimeter, which agreed well with the experiments (fig. S3).

MATERIALS
Hydrogels in Fig. 2F
AMPS hydrogel: AMPS (20 g) (Macklin) was dissolved in 80 g of deionized water; N,N'-methylenebis(acrylamide) (MBAA; Macklin) at 0.031 the weight of AMPS was added as a crosslinker; Irgacure 2959 (Sigma-Aldrich) at 0.01 the weight of AMPS was added as a photoinitiator.

AAm hydrogel: AAm (4.054 g) (Macklin) was dissolved in 30 ml of deionized water. MBAA at 0.0016 the weight of AAm was added as a crosslinker; ammonium persulfate (APS; Sigma-Aldrich) at 0.0017 the weight of AAm was added as a heat initiator; N,N,N',N'-tetramethylethylenediamine (TEMED; Sigma-Aldrich) at 0.0025 the weight of AAm was added as a crosslinking accelerator.

Alginate hydrogel: Alginate (0.676 g) (Aladdin) was dissolved in 30 ml of deionized water.

AAm/alginate hydrogel: AAm (4.054 g) and alginate (0.676 g) were dissolved in 30 ml of deionized water. MBAA at 0.0006 the

weight of AAm was added as a crosslinker; APS at 0.0017 the weight of AAm was added as a heat initiator; TEMED at 0.0025 the weight of AAm was added as a crosslinking accelerator.

Liquid solutions in Fig. 2G

NIPAM hydrogel: NIPAM (4 g) (Macklin) was dissolved in 16 ml of deionized water; MBAA at 0.01 the weight of NIPAM was added as a crosslinker; Irgacure 2959 at 0.01 the weight of NIPAM was added as a PI.

PEGDA hydrogel: PEGDA (4 g) (Sigma-Aldrich) was dissolved in 16 ml of deionized water; Irgacure 2959 at 0.01 the weight of PEGDA was added as a PI.

Ionic liquid: 1-Ethyl-3-methylimidazolium ethyl sulfate (Macklin) was used without any preprocessing.

Photosensitive resin: Photosensitive resin (Ransheng 6002-395) was used without any preprocessing.

Hydrogels in Fig. 5

AAm polymerized by UV: AAm (4 g) and LiCl·H₂O (4 g) (Macklin) were dissolved in 16 ml of deionized water. MBAA at 0.0016 the weight of AAm was added as a crosslinker; Irgacure 2959 at 0.01 the weight of AAm was added as a PI. The UV intensity is 100 mW/cm² in the curing process. LiCl·H₂O was used to decrease the volatilization of the solution (*40*).

NIPAM hydrogel: NIPAM (4 g) was dissolved in 16 ml of deionized water. MBAA at 0.01 the weight of NIPAM was added as a crosslinker; Irgacure 2959 at 0.01 the weight of AAm was added as a PI.

Bonding treatments for VHB material with hydrogel and LED pins with hydrogel

Benzophenone (10 g) (Macklin) was dissolved in 90 g of ethanol. The VHB (3 M) tape was soaked in 10 weight % benzophenone ethanol solution for 10 s. Next, the VHB material was washed by acetone, ethanol, and deionized water sequentially to remove excess benzophenone on its surface.

3-(Trimethoxysilyl)propyl methacrylate (TMASPA) (2 g) (Sigma-Aldrich) was added into 98 g of deionized water; acetic acid was added to tune the pH of the solution to 4. The solution was stored for 2 hours before use. The LED pins were first treated with oxygen plasma for 2 min and then soaked in the TMASPA solution for 2 hours. Last, they were washed with acetone, ethanol, and deionized water sequentially to remove excess TMASPA on its surface.

Mechanical characterization

The 180° peeling tests were conducted with a Shimadzu AGS-X testing machine. Two layers of hydrogel were polymerized sequentially through our printing system. Two polyethylene terephthalate films were bonded to the upper and lower surfaces of the hydrogel sample to constrain the deformation of the sample. The sample was fixed to the two clamps of the testing machine and peeled at a speed of 0.5 mm/s. The interlaminar strength can be calculated by $\Gamma = 2F/w$, where F is the average force between two clamps when two layers of hydrogel are peeled off stably and w is the width of the sample. The fracture strength of the bulk hydrogel material was measured by precutting a crack and testing with the same machine.

The cyclic loading tests of the LED belt were conducted with a Shimadzu AGS-X testing machine. The belt was fixed to the clamps of the testing machine with an effective distance of 60 mm. The loading speed was 6 mm/s. The LED belt was stretched to twice its original length and then unloaded at the same speed to its original length. The loading and unloading were repeated 100 times. During cycling, the luminance of the LED did not change.

SUPPLEMENTARY MATERIALS

Supplementary material for this article is available at http://advances.sciencemag.org/cgi/content/full/5/3/eaau8769/DC1

Fig. S1. Distributions of electric fields simulated using COMSOL.
Fig. S2. Calculation of the free energy for the system.
Fig. S3. Characteristic size of the PLEEC panel.
Fig. S4. Working process of the solution-adding unit.

REFERENCES AND NOTES

1. S. J. Buwalda, K. W. M. Boere, P. J. Dijkstra, J. Feijen, T. Vermonden, W. E. Hennink, Hydrogels in a historical perspective: From simple networks to smart materials. *J. Control. Release* **190**, 254–273 (2014).

2. P. Chawla, A. R. Srivastava, P. Pandey, V. Chawla, Hydrogels: A journey from diapers to gene delivery. *Mini Rev. Med. Chem.* **14**, 154–167 (2014).

3. Y. Qiu, K. Park, Environment-sensitive hydrogels for drug delivery. *Adv. Drug Deliv. Rev.* **53**, 321–339 (2001).

4. K. Y. Lee, D. J. Mooney, Hydrogels for tissue engineering. *Chem. Rev.* **101**, 1869–1879 (2001).

5. T. Billiet, M. Vandenhaute, J. Schelfhout, S. Van Vlierberghe, P. Dubruel, A review of trends and limitations in hydrogel-rapid prototyping for tissue engineering. *Biomaterials* **33**, 6020–6041 (2012).

6. J. Li, A. D. Celiz, J. Yang, Q. Yang, I. Wamala, W. Whyte, B. R. Seo, N. V. Vasilyev, J. J. Vlassak, Z. Suo, D. J. Mooney, Tough adhesives for diverse wet surfaces. *Science* **357**, 378–381 (2017).

7. D. J. Beebe, J. S. Moore, J. M. Bauer, Q. Yu, R. H. Liu, C. Devadoss, B.-H. Jo, Functional hydrogel structures for autonomous flow control inside microfluidic channels. *Nature* **404**, 588–590 (2000).

8. A. Sidorenko, T. Krupenkin, A. Taylor, P. Fratzl, J. Aizenberg, Reversible switching of hydrogel-actuated nanostructures into complex micropatterns. *Science* **315**, 487–490 (2007).

9. J. P. Gong, Y. Katsuyama, T. Kurokawa, Y. Osada, Double-network hydrogels with extremely high mechanical strength. *Adv. Mater.* **15**, 1155–1158 (2003).

10. J.-Y. Sun, X. Zhao, W. R. K. Illeperuma, O. Chaudhuri, K. H. Oh, D. J. Mooney, J. J. Vlassak, Z. Suo, Highly stretchable and tough hydrogels. *Nature* **489**, 133–136 (2012).

11. G. Gerlach, M. Guenther, J. Sorber, G. Suchaneck, K.-F. Arndt, A. Richter, Chemical and pH sensors based on the swelling behavior of hydrogels. *Sensor. Actuat. B Chem.* **111–112**, 555–561 (2005).

12. W. R. K. Illeperuma, J.-Y. Sun, Z. Suo, J. J. Vlassak, Force and stroke of a hydrogel actuator. *Soft Matter* **9**, 8504–8511 (2013).

13. S. E. Bakarich, R. Gorkin III, M. in het Panhuis, G. M. Spinks, 4D printing with mechanically robust, thermally actuating hydrogels. *Macromol. Rapid Commun.* **36**, 1211–1217 (2015).

14. C. Keplinger, J.-Y. Sun, C. C. Foo, P. Rothemund, G. M. Whitesides, Z. Suo, Stretchable, transparent, ionic conductors. *Science* **341**, 984–987 (2013).

15. J.-Y. Sun, C. Keplinger, G. M. Whitesides, Z. Suo, Ionic skin. *Adv. Mater.* **26**, 7608–7614 (2015).

16. C.-C. Kim, H.-H. Lee, K. H. Oh, J.-Y. Sun, Highly stretchable, transparent ionic touch panel. *Science* **353**, 682–687 (2016).

17. C. Larson, B. Peele, S. Li, S. Robinson, M. Totaro, L. Beccai, B. Mazzolai, R. Shepherd, Highly stretchable electroluminescent skin for optical signaling and tactile sensing. *Science* **351**, 1071–1074 (2016).

18. S. Hong, D. Sycks, H. F. Chan, S. Lin, G. P. Lopez, F. Guilak, K. W. Leong, X. Zhao, 3D printing of highly stretchable and tough hydrogels into complex, cellularized structures. *Adv. Mater.* **27**, 4035–4040 (2015).

19. D. M. Kirchmajer, R. Gorkin III, M. in het Panhuis, An overview of the suitability of hydrogel-forming polymers for extrusion-based 3D-printing. *J. Mater. Chem. B* **3**, 4105–4117 (2015).

20. A. A. Pawar, G. Saada, I. Cooperstein, L. Larush, J. A. Jackman, S. R. Tabaei, N.-J. Cho, S. Magdassi, High-performance 3D printing of hydrogels by water-dispersible photoinitiator nanoparticles. *Sci. Adv.* **2**, e1501381 (2016).

21. F. Zhu, L. Cheng, J. Yin, Z. L. Wu, J. Qian, J. Fu, Q. Zheng, 3D printing of ultratough polyion complex hydrogels. *ACS Appl. Mater. Interfaces* **8**, 31304–31310 (2016).

22. T. Q. Huang, X. Qu, J. Liu, S. Chen, 3D printing of biomimetic microstructures for cancer cell migration. *Biomed. Microdevices* **16**, 127–132 (2014).

23. L. A. Hockaday, K. H. Kang, N. W. Colangelo, P. Y. C. Cheung, B. Duan, E. Malone, J. Wu, L. N. Girardi, L. J. Bonassar, H. Lipson, C. C. Chu, J. T. Butcher, Rapid 3D printing of

anatomically accurate and mechanically heterogeneous aortic valve hydrogel scaffolds. *Biofabrication* **4**, 035005 (2012).

24. J. Odent, T. J. Wallin, W. Pan, K. Kruemplestaedter, R. F. Shepherd, E. P. Giannelis, Highly elastic, transparent, and conductive 3D-printed ionic composite hydrogels. *Adv. Funct. Mater.* **27**, 1701807 (2017).

25. K. Tian, J. Bae, S. E. Bakarich, C. Yang, R. D. Gately, G. M. Spinks, M. in het Panhuis, Z. Suo, J. J. Vlassak, 3D printing of transparent and conductive heterogeneous hydrogel–elastomer systems. *Adv. Mater.* **29**, 1604827 (2017).

26. R. L. Truby, J. A. Lewis, Printing soft matter in three dimensions. *Nature* **540**, 371–378 (2016).

27. V. Chan, P. Zorlutuna, J. H. Jeong, H. Kong, R. Bashir, Three-dimensional photopatterning of hydrogels using stereolithography for long-term cell encapsulation. *Lab Chip* **10**, 2062–2070 (2010).

28. B. D. Fairbanks, M. P. Schwartz, C. N. Bowman, K. S. Anseth, Photoinitiated polymerization of PEG-diacrylate with lithium phenyl-2,4,6-trimethylbenzoylphosphinate: Polymerization rate and cytocompatibility. *Biomaterials* **30**, 6702–6707 (2009).

29. L. Ouyang, C. B. Highley, W. Sun, J. A. Burdick, A generalizable strategy for the 3D bioprinting of hydrogels from nonviscous photo-crosslinkable inks. *Adv. Mater.* **29**, 1604983 (2017).

30. F. Mugele, J.-C. Baret, Electrowetting: From basics to applications. *J. Phys. Condens. Matter* **17**, R705–R774 (2005).

31. G. Lippmann, *Relations Entre les Phénomènes Électriques et Capillaires* (Gauthier-Villars, 1875).

32. L. Chen, L. Zhuang, P. Deshpande, S. Chou, Novel polymer patterns formed by lithographically induced self-assembly (LISA). *Langmuir* **21**, 818–821 (2005).

33. M.-Y. Chiang, Y.-W. Hsu, H.-Y. Hsieh, S.-Y. Chen, S.-K. Fan, Constructing 3D heterogeneous hydrogels from electrically manipulated prepolymer droplets and crosslinked microgels. *Sci. Adv.* **2**, e1600964 (2016).

34. D. Tian, Q. Chen, F.-Q. Nie, J. Xu, Y. Song, L. Jiang, Patterned wettability transition by photoelectric cooperative and anisotropic wetting for liquid reprography. *Adv. Mater.* **21**, 3744–3749 (2009).

35. M. Dhindsa, J. Heikenfeld, S. Kwon, J. Park, P. D. Rack, I. Papautsky, Virtual electrowetting channels: Electronic liquid transport with continuous channel functionality. *Lab Chip* **10**, 832–836 (2010).

36. P. C. Marr, A. C. Marr, Ionic liquid gel materials: Applications in green and sustainable chemistry. *Green Chem.* **18**, 105–128 (2016).

37. C. Yang, Z. Suo, Hydrogel ionotronics. *Nat. Rev. Mater.* **3**, 125–142 (2018).

38. H. Yuk, T. Zhang, S. Lin, G. A. Parada, X. Zhao, Tough bonding of hydrogels to diverse non-porous surfaces. *Nat. Mater.* **15**, 190–196 (2016).

39. H. Yuk, T. Zhang, G. A. Parada, X. Liu, X. Zhao, Skin-inspired hydrogel–elastomer hybrids with robust interfaces and functional microstructures. *Nat. Commun.* **7**, 12028 (2016).

40. Y. Bai, B. Chen, F. Xiang, J. Zhou, H. Wang, Z. Suo, Transparent hydrogel with enhanced water retention capacity by introducing highly hydratable salt. *Appl. Phys. Lett.* **105**, 151903 (2014).

Citation: J. Wang, T. Lu, M. Yang, D. Sun, Y. Xia, T. Wang, Hydrogel 3D printing with the capacitor edge effect. *Sci. Adv.* **5**, eaau8769 (2019).

Science Advances

Hydrogel 3D printing with the capacitor edge effect

Jikun Wang, Tongqing Lu, Meng Yang, Danqi Sun, Yukun Xia and Tiejun Wang

ARTICLE TOOLS	http://advances.sciencemag.org/content/5/3/eaau8769
SUPPLEMENTARY MATERIALS	http://advances.sciencemag.org/content/suppl/2019/03/18/5.3.eaau8769.DC1
REFERENCES	This article cites 39 articles, 7 of which you can access for free http://advances.sciencemag.org/content/5/3/eaau8769#BIBL
PERMISSIONS	http://www.sciencemag.org/help/reprints-and-permissions

Use of this article is subject to the Terms of Service